Available online at www.sciencedirect.com

ScienceDirect

Procedia Engineering 10 (2011) 124–129

Engineering Procedia

ICM11

The Microstructural Effects on the Mechanical and Thermal Properties of Pulsed Electric Current Sintered Cu-Al_2O_3 Composites

R. Ritasalo[a]*, X.W. Liu[a], O. Söderberg[a], A. Keski-Honkola[a], V. Pitkänen[a], S-P. Hannula[a]

[a]*Aalto University School of Chemical Technology, POB 16200, FI-00076, Aalto, Espoo, Finland*

Abstract

In this work, the influences of the microstructure on the mechanical and thermal properties of pulsed electric current sintered (PECS) Cu-Al_2O_3 composites are investigated. The process parameters were optimized for four different grades of composite powders to obtain dense samples (98-99.6 %T.D.). Higher hardness and better thermal stability were attained to the samples compacted from commercial internally oxidized (IO) powders than to the compacts made from the chemically synthesised experimental powders. This difference was attributed to the distribution and size of Al_2O_3-particles in the two types of composites. The CTE values of all the compacts were between 17 and 20 x 10^{-6} K^{-1} (370-770 K). The results show that PECS can be used to produce dense high quality Cu-Al_2O_3 composites.

Selection and peer-review under responsibility of ICM11

Keywords: Cu-Al_2O_3; Copper composites; Pulsed electric current sintering (PECS); Microstructure; Nanoindentation; Thermal stability; CTE

1. Introduction

Copper is widely used as an electrical conductor because of its high electrical and thermal conductivity, but it has low tensile and yield strength [1-3]. To solve this problem, copper has been strengthened by several different ways. Conventional methods such as cold working and precipitation hardening as well as solid solution hardening, which lower thermal conductivity, are not suitable for high-temperature applications [1,3-6]. There the primary attention is in dispersion strengthening (DS) of copper, i.e. in copper based metallic matrix composites (MMC). In the *ex-situ* MMCs the scale of the reinforcing phase is limited by the starting powder size and by the wettability between the reinforcements and the matrix [7,8]. This has led to the development of *in-situ* MMCs, in which the reinforcements are formed within the metallic matrix during the composite fabrication, e.g. via internal oxidation (IO) [1-3,6-15], mechanical alloying (MA) [13-18] or chemical routes [19,20].

The major requirements for the dispersed particles are thermodynamic and chemical stability, low diffusivity and low solubility in the copper matrix, high interfacial energy of the particle-matrix interface, and

* Corresponding author. Tel.: +358-9-47022671; fax: +358-9-47022677.
E-mail address: riina.ritasalo@ttk.fi.

Selection and peer-review under responsibility of ICM11 doi:10.1016/j.proeng.2011.04.023

coefficients of the thermal expansion (CTE) of the matrix and particles that are close to each other [4,5]. Finely dispersed Al_2O_3 particles can fulfill these requirements. When interparticle distance, distribution, volume fraction and particle size are properly adjusted [1,4,7,10,15] these materials have many potential high-temperature applications including frictional brake parts, electrodes, electrical conductors, heat exchangers etc. [1,7,9,10]. Thus, *in-situ* Cu-Al_2O_3 MMCs' have been studied in numerous investigations and reviews [4,5]; mainly concentrating on preparation [10,12-20], strengthening mechanisms [3,6,11,18,21,22], or the thermal stability [2-3,6,10-15,17-18, 23-25].

Ferkel [18] evaluated the hardness and thermal stability of laser-generated and subsequently mixed or milled and extruded Cu - 3 vol.% Al_2O_3 composites. Extruded composite showed finer microstructure when the powder was milled instead of mixing, the dispersoids were found also inside copper grains, the hardness was higher (1.3 GPa vs. 0.9 GPa) and softening as well as the grain growth were restricted below 1173 K. Hwang and Hahn [21,22] estimated the Hall-Petch and Orowan effects in nanocrystalline Cu - 4 vol.% Al_2O_3 prepared by cryo-milling and hot pressing at 1123 K. They suggested that the major contribution to the total strengthening is because of grain size effect. Rajkovic *et al.* [13-15] have compared the preparation and thermal stability of Cu with different contents and sizes of Al_2O_3 dispersoids, prepared by MA or by IO and hot pressing (HP) under 35 MPa pressure at 1073 K for 1 h. IO-Al_2O_3 was much finer than that prepared with MA, consequently effectively preventing the grain growth, providing higher strength and superior thermal stability below 1073 K. Tian *et al.* [3] studied microstructure, strengthening mechanisms, and properties of an internally oxidized and cold compacted nano-Al_2O_3 DS copper composites at elevated temperatures. The softening resistance of Cu - 0.5 vol.% Al_2O_3 remained up to about 1073 K as compared to that of Cu (673 K). Strength at elevated temperature was mainly attributed to strong pinning of grain boundaries and sub-grain boundaries by about 20 - 50 nm Al_2O_3-dispersoids, which were found inside the copper grains.

PECS based on the pulsed high DC current has resulted in improvements in processing of a variety of nanostructured materials [26]. Although a lot of works have been done on Cu-Al_2O_3 composites, studies on PECS processed nano-Al_2O_3-Cu are rare. In the only PECS study of copper Al_2O_3-composite [27] found by the authors, powder mixtures of Cu + 0-1.5 wt.% α - Al_2O_3 (150 nm) were prepared using MA followed by spheroidizing by hybridization. The mixtures were then compacted using PECS and HP. Bending strength of 597 MPa, density of 99 % of T.D. and electrical conductivity of 88 % IACS were achieved for 1 wt.% Al_2O_3. In the present study, optimization of PECS process for two types of Cu-Al_2O_3 composites is carried out and the properties of the obtained composites are characterized to demonstrate the correlation between microstructural features and mechanical / nanomechanical and thermal properties of the composites.

2. Materials and Experiments

Four Cu-Al_2O_3 composite powders were used for the compactions: (**A**) commercial, internally oxidised Cu - 0.5 wt.% Al_2O_3 powder (UNS-C15725); (**B**) commercial, internally oxidised Cu - 1.1 wt.% Al_2O_3 powder (UNS-C15760); (**C**) experimental Cu - 1.1 wt.% Al_2O_3 composite powder prepared via chemical route; and (**D**) experimental Cu - 2.75 wt.% Al_2O_3 composite powder prepared also via chemical route. The latter two Cu-Al_2O_3 composite powders have been prepared by adding Cu_2O to aqueous solution of aluminium nitrate and then preferentially reducing Cu_2O at 673 K by hydrogen. According to Fig. 1 showing the morphologies of the powders the particle size distribution is noticeably wider in the commercial powders (mostly between 5 - 100 μm) than in the experimental powders (mostly between 5 - 15 μm). In all the powders fine Al_2O_3 particles were detected on the surface of the copper particles, and in the commercial powders fine (about 30 to 300 nm sized) Al_2O_3 particles also inside the particles.

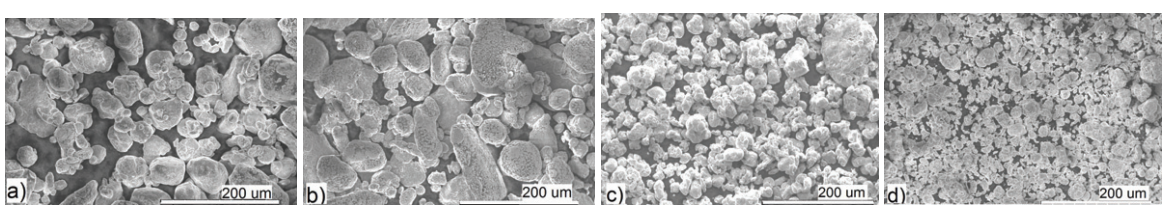

Fig. 1. Morphology of the studied powders (a) A; (b) B; (c) C; (d) D. The scale bar is 200 microns.

The structure and morphology of the initial powders were studied by θ-2θ X-ray diffraction, XRD (Philips PW3830) and scanning electron microscopy, SEM (Hitachi FE-SEM S-4700 equipped with Inca EDS). The PECS process was carried out using FCT HP D 25 equipment. In all of the tests, the current pulse-pause ratio was 10:5 ms, the heating rate was 75 K/min, and the holding time was 6 min. Sintering temperatures were varied between 1073 and 1223 K while the pressure was 50 MPa or 100 MPa. To optimize the process parameters, 3 to 8 experiments for each powder were needed. After compaction the samples were ground with sand grit papers up to 1200 mesh and their density measured using the Archimedes method. For mechanical characterization, the samples were further polished with diamond paste down to 1 μm. After polishing, Vickers hardness (HV1) was measured with a Z323 hardness tester (Zwick&Co.KG). An average of five measurements is taken for each composite as the bulk value. In addition, nanoindentation was used to investigate the mechanical response of the composites at sub-micron scale. A TriboIndenter nanomechanical system (Hysitron Inc.) was used in the measurement with a Berkovich indenter. The indentation cycle was set as 25 μN/s loading / unloading rate, 250 μN maximum load and 5s holding before unloading. Multiple indents were performed at three to five locations on the sample surface in order to gain high statistical significance in data analysis.

A set of techniques including XRD, transmission electron microscopy (FEG-TEM Tecnai F20), STEM imaging, selected area diffraction pattern (SADP) and energy dispersive X-ray (EDX) spectroscopy were used to investigate the phase composition and microstructure of the sintered composites. To evaluate the thermal stability, annealing treatments in argon atmosphere were performed at two temperatures: 973 K for 3 h and 1023 K for 1 h with 10 K/min heating / cooling. PECS compacted pure copper sample was used as a reference. Micro- and macrohardness (HV1 and HV10) values were measured before and after the heat-treatments. A Netzch DIL 402C device was used in the CTE measurement in which the samples were annealed for 5 minutes at 973 K in argon atmosphere with the heating/cooling rate as 10 K/min.

3. Results

The optimized process temperature and pressure for achieving dense compacts as well as their relative density and hardness are shown in Table 1. In calculating the relative density of the compacts theoretical density (T.D.) of 8.86 g/cm^3 and 8.81 g/cm^3 was taken for sample 1 and 2, respectively [7]. For sample 3 and 4, the T.D.'s were calculated by taking 3.95 g/cm^3 as the density of the Al_2O_3 and 8.96 g/cm^3 for the Cu [15].

Fig. 2 shows the microstructures of the compacts after PECS process with the small inserts in the pictures indicating Al_2O_3-particles on samples. The average grain size for samples 1 and 2 was 25 μm (with wide grain size distribution between 2 and 100 μm) and for sample 3 and 4 it was 10 μm (with narrower grain size distribution between 5 and 15 μm). Due to the small amount of Al_2O_3 it could not be detected by XRD from the powders or the samples. Neither was cuprite or other oxides of copper detected, so possible oxidation of copper in the process was below the detection limit.

Table 1. The sintering parameters applied for the studied samples and their properties after PECS.

	1	2	3	4
Sintering temperature (K)	1173	1223	1073	1173
Sintering Pressure (MPa)	100	100	50	50
Relative density (%)	98.6±0.1	99.1±0.1	98.7±0.6	99.6±0.1
Hardness (GPa)	1.22±0.17	1.58±0.06	0.78±0.01	0.93±0.01

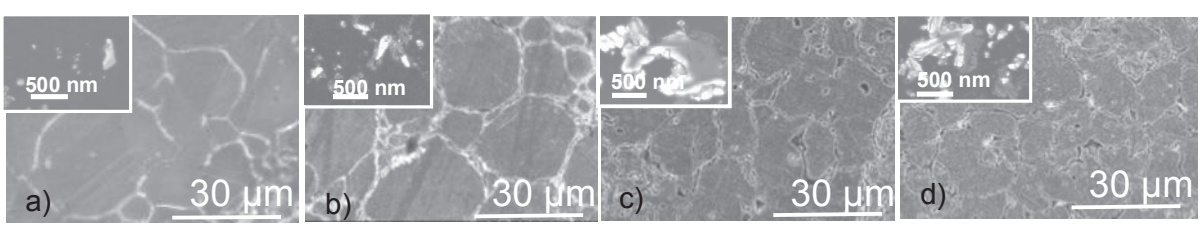

Fig. 2. The microstructures of the samples. Inserts at the left corner show Al_2O_3-particle distributions for (a) 1; (b) 2; (c) 3; and (d) 4.

Fig. 3a is an example of scanning probe microscopy (SPM) image for sample 2 demonstrating the indent marks and showing also some nano- to submicron sized alumina particles (bright spots) on sample surface. In

Fig. 3b, the averaged nanohardness has a standard deviation of 0.5 GPa while the averaged elastic modulus has a standard deviation of 20 GPa. Samples 1 and 2 compacted from the commercial powders are harder than those made from the experimental powder.

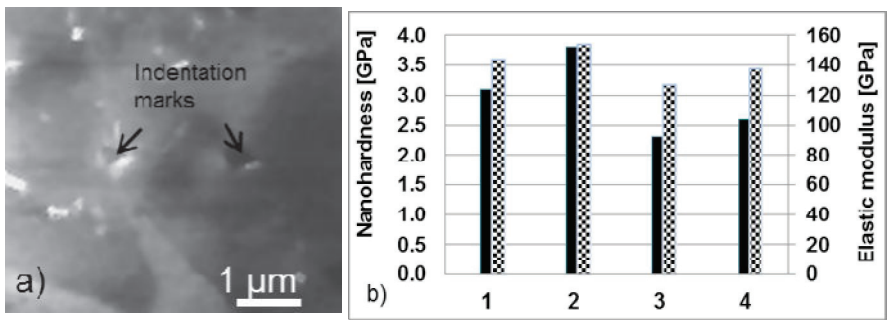

Fig. 3. (a) The SPM image on the sample 2; and (b) the average nanohardness (left side bars) and elastic modulus (right side bars) values for the samples 1, 2, 3 and 4.

Figs. 4a and b are STEM micrographs of the sample 2 showing fine nano- and submicron sized alumina particles in copper matrix. The selected area diffraction (SAD) pattern indicates gamma-alumina (γ-Al_2O_3) [28]. Fig. 4c shows the STEM micrograph of the sample 3 with SAD; indicating agglomerates of γ-Al_2O_3.

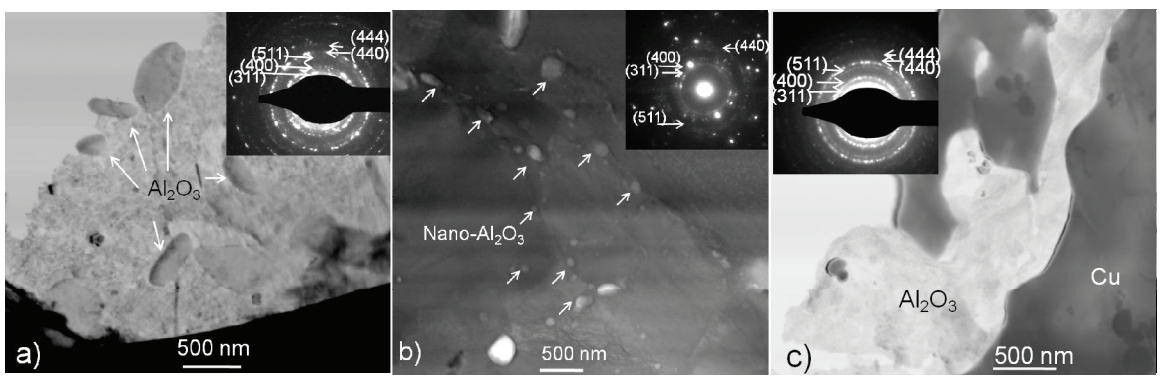

Fig. 4. (a) and (b) STEM micrographs of the sample 2 with SAD; (c) STEM micrograph of the sample 3 with SAD.

The microhardness values for all four samples and reference copper before and after heat-treatments (at 973 K for 3 h and at 1023 K for 1 h) are shown in Fig. 5a as a function of Al_2O_3 content. The corresponding macrohardness values were at the same level, the difference being ± 0.05 GPa. The CTE values of the different compacts within the temperature range of 293 to 973 K are shown in Fig. 5b.

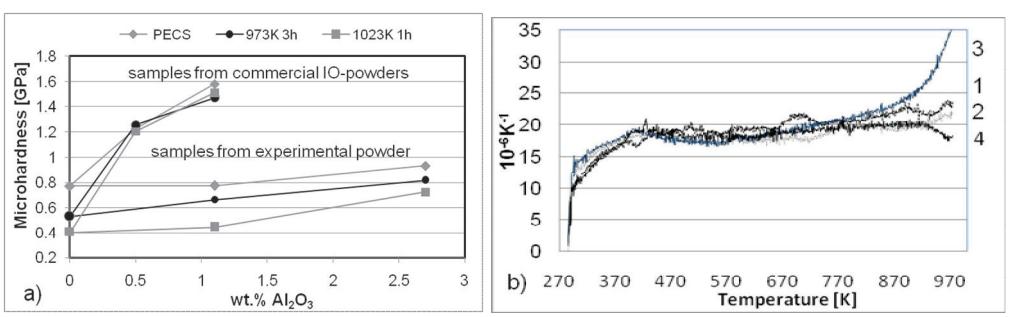

Fig. 5. (a) The hardness dependence on the Al_2O_3 content before and after the heat-treatments at 973 K for 3 h and at 1023 K for 1 h; (b) The CTE of the compacts in the temperature region of 293-973K.

4. Discussion

Dense samples (more than 98.5 % of T.D.) were achieved from all the starting powders after process optimization. Much higher nano- and microhardness values were measured for the compacts made from the commercial powders as compared to those made from experimental powders synthesized by a chemical method. E.g., sample 2 has two times higher microhardness (1.58 GPa) than sample 3 (0.78 GPa), even though they contain the same amount (1.1 wt.%) of alumina. On the other hand the corresponding nanohardness values were 3.8 and 2.3 GPa. The ratio of the nanohardness values is clearly smaller indicating that the local difference within the grains of the two materials is less than the overall hardness differences of the materials. This is somewhat surprising since alumina particles seem to be more evenly distributed in the compacts made from commercial powders. The differences in nano- and microhardness values may arise in addition to the intrinsic property variation from point to point over the sample surface from several other reasons including the different scales applied, indentation size effects, and existence of hardened surface layers. Because nanohardness represents material property of small volumes, it is sensitive to local microstructural features such as local particle densities and even surface roughness. This also explains the larger data scattering in nanoindention.

The overall hardness difference between the compacts can be attributed to the size and distribution of alumina in the compacts. The finer size and more even distribution of Al_2O_3 in compacts made from the commercial powders (A and B) results in a clearly higher hardness than in compacts made from experimental powders (C and D) in which the alumina is coarser and more segregated at the grain boundaries. This was verified with SEM and TEM studies, which showed larger regions of alumina in the samples 3 and 4, whereas the nano- and submicron sized alumina was observed in the samples 1 and 2 (Figs. 2 and 4). Our results are in line with those obtained by conventional compaction methods [13-15,18]. The small and evenly distributed hard Al_2O_3-particles act as reinforcing phases and become obstacles to the movement of dislocations [3,15,18,20]. Generally, the Orowan's strengthening (nano-Al_2O_3 can increase the resistance of dislocation movement and restrain the grain growth) and/or Hall-Petch effect (grain size strengthening) are thought to explain the high strength of these composites [6,16,18,21,22,29]. Even though the grain size of the Cu is smaller in the compacts made from experimental Cu-powder (C and D), the hardness of the compacted samples 3 and 4 is much lower due to larger Al_2O_3 size and consequently larger interparticle distance. It is noteworthy to point out that the hardness values in literature show quite much variation depending on the powder processing and compaction methods, as well as amount and size of alumina; i.e., values from 0.9 to 1.82 GPa have been reported [1,3,6,18,25]. Our results are within this range.

Because DS copper contains small amounts of aluminium oxide as discreet particles in essentially pure copper matrix, its physical properties e.g. modulus of elasticity and CTE closely resemble those of pure copper [1,7]. The modulus values reported are between 115 [1,7] and 130 GPa [7] for both the copper and Cu-Al_2O_3. We measured slightly higher modulus values for the samples 1 and 2 (Fig. 3b), but regarding the scatter of about ± 20 GPa, our results seems to be in line with the values reported. CTE in our measurements (Fig. 5b) was less than 17 x 10^{-6} K^{-1} between 270 - 370 K, 17 - 20 x 10^{-6} K^{-1} between 370 - 770 K and above this temperature about 20 x 10^{-6} K^{-1} or more. The expansion is largest for the sample 3; the value reaching 35 x 10^{-6} K^{-1} at 970 K indicating poor properties at high temperatures. Our CTE values are in agreement with those found from the literature; from 16.6 x 10^{-6} K^{-1} [1,7] to 20.4 x 10^{-6} K^{-1} [7,10] for Cu-Al_2O_3, and from 17.7 x 10^{-6} K^{-1} [1,7] to 20 x 10^{-6} K^{-1} [30] for copper.

The samples compacted from the commercial composite powders (1 and 2) retain the high hardness also after annealing at 973 - 1023 K (Fig. 5a). On the other hand, compact 4 made from the experimental powder having 2.75 wt.% Al_2O_3 show only minor hardness drop after 1 hour annealing at 1023 K, while the hardness decrease of 1.1 wt.% alumina composite (the compact 3) is about the same as for reference copper compact. The softening temperatures (the temperature where material rapidly loses its strength [3,23]) reported for copper are between 523 K [23] and 673 K [3] and for Cu-Al_2O_3 composites from 773 K [25] to 1273 K [12] depending on the size, distribution and amount of alumina. Also, the high-temperature properties i.e. thermal stability greatly depends on the content, distribution and size of alumina [6,13-15,17-18,24]. The finely dispersed particles inhibit the sliding of grain and sub-grain boundaries, retard strongly recrystallization, and result in texture strengthening at high temperatures [3]. Coarse alumina particles have less pinning effect on grain boundaries, owing to the large spacing and hence the copper grains next and between to these particles can grow more rapidly at high temperatures than those pinned by the fine alumina particles [12]. For this

reason, samples 1 and 2 showed better thermal stability at high temperatures, whereas in sample 3 softening occurred below 973 K and for the sample 4 softening was restricted up to about 973 K. The better hardness and thermal stability of the sample 4 in comparison to the sample 3 resulted from the higher weight percentage of hard Al_2O_3 dispersoids.

5. Conclusions

This study has shown that PECS can be used to produce dense high quality Cu-Al_2O_3 composites having comparable properties to those prepared by conventional methods. Based on the results obtained it is expected that PECS can be used also for processing of very fine-grained Cu-Al_2O_3 composites. The four grades of Cu-Al_2O_3 composite powders used for PECS compaction resulted in materials with distinctly different properties. The highest hardness values were measured for the samples compacted from commercial powders produced by IO. These samples also showed high thermal stability and retained high hardness after three hour annealing at 973 K and one hour annealing at 1023 K. Compactions made from the experimental powders resulted in lower hardness and temperature stability. The reason for the different hardness levels and elevated temperature stability is the difference in the distribution and size of Al_2O_3-dispersoids in the copper matrix. The CTE values of all the compacts despite of different amount and distribution of alumina were between 17 and 20 x 10^{-6} K^{-1} in the temperature range of 370 and 770 K being in good accordance with the values given in the literature for corresponding conventionally processed alloys.

Acknowledgements

This work was supported by Tekes and a consortium of Finnish companies. The Center of New Materials at Aalto University School of Chemical Technology (UMK) and Outotec (Finland) Oyj are also acknowledged.

References

[1] A.V. Nadkarni, J.E. Synk, Metals Handbook, Powder Metallurgy ASM, Metals Park, OH, 1984, p.711.
[2] L. Guobin, S. Jibing, G. Quanmei, and W. Ru, *J. Mater. Process. Tech.* 170 (2005) 336.
[3] B. Tian, P. Liu, K. Song, Y. Li, Y. Liu, F. Ren, and J. Su, *Mater. Sci. Eng. A* 435-436 (2006) 705.
[4] J.R. Groza, *J. Mat. Eng. Perf.* 1 (1992) 113.
[5] J.R. Groza, and J.C. Gibeling, *Mater. Sci. Eng. A* 171 (1993) 115.
[6] J. Lee, Y.C. Kim, S. Lee, S. Ahn, and N.J. Kim, *Met. Mat. Trans. 35A* (2004) 493.
[7] Glidcop, SCM Product Literature 1994, SCM Glidcop product info, cited in http://www.aps.anl.gov/APS_Engineering_Support_Division/Mechanical_Operations_and_Maintenance/Miscellaneous/tech_info/Glidcop/Glidcop.html [06.01.2011]
[8] Z. Shi, and M. Yan, *Appl. Surf. Sci.* 134 (1998) 103.
[9] A.V. Nadkarni, and E. Klar, Strengthening of metals by internal oxidation, USPatent No. 3,779,714 (1973).
[10] A.V. Nadkarni, P. K. Samal, and J.E. Synk, Dispersion strengthened metal composites, USPatent No. 4,752,334 (1988).
[11] A. Afshar, and A. Simchi, *Mater. Sci. Eng. A* 518 (2009) 41.
[12] A. Afshar, and A. Simchi, *Scr. Mater.* 58 (2008) 966.
[13] V. Rajkovic, D. Bozic, and M.T. Jovanovic, *J. Mater. Process. Tech.* 200 (2008) 106.
[14] V. Rajkovic, D. Bozic, and M.T. Jovanovic, *Mater. Design* 31 (2010) 1962.
[15] V. Rajkovic, D. Bozic, and M.T. Jovanovic, *J. Alloys Comp.* 459 (2008) 177.
[16] S.J. Hwang, and J.-H. Lee, *Mater. Sci. Eng. A* 405 (2005) 140.
[17] J. Naser, W. Riehemann, and H. Ferkel, *Mater. Sci. Eng. A* 234-236 (1997) 467.
[18] H. Ferkel, *Nanostr. Mater.* 11 (1999) 595.
[19] E.A. Brocchi, M.S. Motta, I.G. Solórzano, P.K. Jena, and F.J. Moura, *Mater. Sci. Eng. B* 112 (2004) 200.
[20] F. Shehata, A. Fathy, M. Abdelhameed, and S.F. Moustafa, *Mater. Design* 30 (2009) 2756.
[21] S.-I. Hahn, and S.J. Hwang, *J. Alloys Comp.* 483 (2009) 207.
[22] S.J. Hwang, *J. Alloys Comp.* 509 (2011) 2355.
[23] S.H. Liang, and Z.K. Fan, *Acta Metall. Sin.* 12 (1999) 782.
[24] Z. Trojanová, H. Ferkel, P. Lukác, J. Naser, and W. Riehemann, *Scr. Mater.* 40 (1999) 1063.
[25] R.K. Islamgaliev, W. Buchgraber, Y.R. Kolobov, N.M. Amirkhanov, A.V. Sergueeva, K.V. Ivanov, and G.P. Grabovetskaya, *Mater. Sci. Eng. A* 319-321 (2001) 872.
[26] R. Orrù, R. Licheri, A.M. Locci, A. Cincotti, and G. Cao, *Mater. Sci. Eng. R* 63 (2009) 127.
[27] X.-B. Liu, C.-C. Jia, X.-H. Chen, and G.-S. Gai, *J. Iron Steel Res. Int.*14 (2007) 94.
[28] X-ray powder diffraction file, Gamma-alumina JCPDS 50-741.
[29] D.V. Kudashov, H. Baum, U. Martin, M. Heilmaier, and H. Oettel, *Mater. Sci. Eng. A* 378-389 (2004) 768.
[30] F.C Nix, and D. MacNair, *Phys. Rev.* 60 (1941) 597.